High Yield Chemical Vapor Deposition Growth of High Quality Large-Area AB Stacked Bilayer Graphene

Lixin Liu[1,4,†], **Hailong Zhou**[2,†], **Rui Cheng**[1,†], **Woo Jong Yu**[2], **Yuan Liu**[1], **Yu Chen**[1], **Jonathan Shaw**[2], **Xing Zhong**[2], **Yu Huang**[*,1,3], and **Xiangfeng Duan**[*,2,3]

[1]Department of Materials Science and Engineering, University of California, Los Angeles, California 90095 USA

[2]Department of Chemistry and Biochemistry, University of California, Los Angeles, California 90095 USA

[3]California Nanosystems Institute, University of California, Los Angeles, California 90095 USA

[4]Key Laboratory for Magnetism and Magnetic Materials of the Ministry of Education, Lanzhou University, Lanzhou 730000, People's Republic of China

Abstract

Bernal stacked (AB stacked) bilayer graphene is of significant interest for functional electronic and photonic devices due to the feasibility to continuously tune its band gap with a vertical electrical field. Mechanical exfoliation can be used to produce AB stacked bilayer graphene flakes but typically with the sizes limited to a few micrometers. Chemical vapor deposition (CVD) has been recently explored for the synthesis of bilayer graphene but usually with limited coverage and a mixture of AB and randomly stacked structures. Herein we report a rational approach to produce large-area high quality AB stacked bilayer graphene. We show that the self-limiting effect of graphene growth on Cu foil can be broken by using a high H_2/CH_4 ratio in a low pressure CVD process to enable the continued growth of bilayer graphene. A high temperature and low pressure nucleation step is found to be critical for the formation of bilayer graphene nuclei with high AB stacking ratio. A rational design of a two-step CVD process is developed for the growth of bilayer graphene with high AB stacking ratio (up to 90 %) and high coverage (up to 99 %). The electrical transport studies demonstrated that devices made of the as-grown bilayer graphene exhibit typical characteristics of AB stacked bilayer graphene with the highest carrier mobility exceeding 4,000 $cm^2/V \cdot s$ at room temperature, comparable to that of the exfoliated bilayer graphene.

Keywords

bilayer graphene; band gap; AB stacking; chemical vapor deposition; copper foil

Bernal AB stacked bilayer graphene is of significant interest for graphene based field effect transistors (FETs) because of the feasibility to continuously tune its band gap with a vertical electrical field.[1,2] This unusual characteristic of bilayer graphene has attracted considerable

attention for fundamental studies and potential applications in digital electronics and photonics.[1–7] To date, most of the bilayer graphene films are prepared by micromechanical exfoliation from graphite with the sizes often limited to a few micrometers, which has therefore seriously limited its potential for scalable fabrication of electronic and photonic devices.

Recently, chemical vapor deposition (CVD) method has emerged as a potentially effective approach to large area graphene on various transition metal (*e.g.*, nickel and copper) substrates using hydrocarbon gas or solid carbon as the carbon source.[8–16] There are two different mechanisms for the formation of graphene depending on the metal substrates used. For metals with relatively high carbon solubility, such as nickel (~1.3 atom % at 1000 °C), the dissolved carbon atoms at high temperature can precipitate out from the metal surface and form multiple layer graphitic films upon cooling.[10,17,18] On the other hand, low carbon solubility metals (*e.g.*, copper, platinum) show predominately uniform monolayer graphene growth due to a self-limiting effect.[19–22] Graphene with controllable number of layers has been reported to grow on the Ni-Cu alloy substrates by tuning of the growth conditions, but the uniformity of the bilayer graphene is limited due to the non-uniform alloy composition.[23] Additionally, the resulted bilayer graphene often consists of a mixture of randomly stacked and AB stacked bilayer graphene. Therefore, it remains a significant challenge to controllably produce large area bilayer graphene, especially the AB stacked bilayer graphene.

Here we present a systematic study to investigate the growth of bilayer graphene on copper surface with high surface coverage and high AB stacking yield. Specifically, a high H_2/CH_4 ratio gas flow is used in the CVD growth to partially expose Cu surface at the upstream end, which is proven to effectively break the self-limiting effect and enable the direct growth of the second layer graphene on the first layer graphene. Additionally, it was found that a low pressure growth can allow for high yield nucleation of AB stacked bilayer graphene. With this discovery, we have developed a two-step low pressure CVD (LPCVD) process to grow large-area AB stacked bilayer graphene. High coverage (up to 99%) and high AB stacking ratio (up to 90%) bilayer graphene sheets with carrier mobility up to 4,400 $cm^2/V \cdot s$ are achieved through the rational design of synthetic process. Our study will help promote the understanding of the growth mechanism of the bilayer graphene and its application for functional electronic devices.

RESULTS AND DISCUSSION

The CVD growth of graphene on Cu substrate is typically controlled by a self-limiting process: Cu substrate catalyzes the cracking of carbon source (*e.g.* CH_4) and the formation of a single layer graphene on its surface. With a low H_2/CH_4 ratio (*e.g.*, 0.06) gas flow,[20] a nearly continuous monolayer of graphene is formed on Cu substrate, the catalytic behavior of the Cu is passivated and prevents the further decomposition of the carbon source molecules for the continued growth of multilayer graphene. As a result, bilayer graphene and particularly large area bilayer graphene is often not readily achievable due to this self-limiting process. To enable the continued growth of large-area bilayer graphene, we have employed a much higher H_2/CH_4 ratio (*e.g.*, 40) gas flow in the CVD growth process to partially expose the upstream Cu surface to break the self-limiting effect.

For a typical growth process, a 1.5 × 6 cm size of 25 μm thick Cu foil was loaded into a 1-inch quartz tube inside a horizontal LPCVD chamber. A gas mixture of H_2 and diluted CH_4 (500 ppm in Ar) with flow rate of H_2/CH_4 = 10/500 sccm was flowed across the Cu substrate at a temperature of 1050 °C under pressure of 5 mbar for 1hour (see methods section for details). The corresponding H_2/CH_4 (pure) ratio is 40. In this way, bilayer

graphene were epitaxially grown on downstream monolayer with the carbon fragments continuously supplied from the uncovered upstream Cu gaps in the LPCVD system (Figure 1a). Bilayer graphene are observed throughout the surface of the entire Cu foil. The variation of the bilayer coverage can be seen in Figures S1 and S2. Figure 1b, c show representative scanning electron microscopy (SEM) images of the transferred graphene located at upstream end and center of the Cu substrate respectively. At the upstream end (~ 5 mm length from head), the Cu surface is partially covered with monolayer and bilayer graphene with some exposed Cu surface (gap) between different graphene domains (Figure 1b and S1). At the downstream end, the Cu substrate is fully covered with continuous monolayer graphene and with large hexagonal domains of bilayer graphene (Figure 1c and S1). The area coverage of the bilayer graphene exceeds 40 % after 1 hour growth with a typical domain size around 20 μm in lateral dimension.

Hydrogen (H_2) is believed to play two important roles in the graphene growth: as a cocatalyst for dehydrogenation of CH_4 for graphene growth and as an etching agent to control the size and morphology of graphene domains.[24,25] The ultimate graphene size and morphology depends on the equilibrium between graphene growth and hydrogen etching. Therefore, the amount of hydrogen is a most critical factor determining the formation of bilayer graphene here. A relatively high H_2/CH_4 ratio can saturate the lateral growth rate of the graphene films to leave uncovered catalytically active Cu surface.[25,26] Briefly, CH_4 precursor and H_2 can be decomposed on the Cu surface to form active CH_4^* (CH_3^*, CH_2^*, and CH^*) and hydrogen atoms, which will bond on the edge of graphene nuclei and eventually lead to the growth of graphene through the dehydrogenation process. Meanwhile, hydrogen atoms can etch graphene carbonaceous edge and form CH_x^* species during the growth. The balance between the growth and etching can result in a saturation of graphene growth. Consequently, a high partial pressure of hydrogen can inhibit graphene domain growth to leave uncovered and catalytically active Cu surface at the upstream end. The continued decomposition of CH_4 on the uncovered Cu area or hydrogen etching of graphene broken edges produces small carbon fragments that can get desorbed from the copper surface and flow downstream, leading to a higher concentration of active carbon source there and contributing to the continued graphene growth to form fully covered graphene surface. Furthermore, the continued supply of small carbon fragments from upstream can enable continued bilayer graphene growth downstream.

The bilayer graphene domains nucleate simultaneously on the monolayer, as shown in Figure 2a. The domain density of bilayer graphene decreases slightly compared to the first layer (1160/mm^2 *vs.* 1300/mm^2). Interestingly, the hexagonal second layer domains typically show a one-to-one relationship with the underlying six-fold symmetric lobe-like first layer domains. The overlapped centers of these two domains indicate the mono- and bilayer graphene tend to nucleate at the same locations, such as step edges, folds, or other imperfections on the Cu foil.[27] Furthermore, the total area of the bilayer coverage increases with increasing growth duration, while the domain density is statistically constant after the initial nucleation stage (Figure S3). Raman spectroscopy was employed to evaluate the quality and layer number of the graphene. In the three Raman spectra (Figure 2b), the peaks centered at ~ 1585 cm^{-1} and ~ 2690 cm^{-1} correspond to the G and 2D bands of the graphene, respectively. The characteristic features in Raman spectra suggest that there are three different graphene materials: AB stacked bilayer graphene, disoriented or randomly stacked bilayer graphene, and monolayer graphene. In particular, the full width at half maximum (FWHM) of 2D band peak is ~ 56 cm^{-1} for the AB stacked bilayer graphene (Figure 2b, red line), distinct from ~ 31 cm^{-1} for disoriented bilayer (Figure 2b, black line) and ~ 37 cm^{-1} for the monolayer (Figure 2b, blue line). The intensity ratio of I_{2D}/I_G for AB stacked bilayer graphene is ~ 1.2, significantly lower than the ratio of ~ 4.5 for disoriented

bilayer and ~ 2.5 for monolayer graphene. In this way, Raman spectra can be used as a reliable way to distinguish the number of layers and the stacking order of the graphene.

The morphologies of the AB stacked and disoriented bilayer graphene in the initial growth stage are further studied, as shown in Figure 2c and 2d. The first layer domains always show six-fold lobes, typically with small hexagonal bilayer domains locate at their centers. In Figure 2c, the frequent observation of zero-rotation relationship between the first layer lobe and the second layer hexagon suggests a possible fixed stacking order, which is confirmed by Raman studies as the lowest energy configuration of AB-stacking order (the red curve in the Figure 2b). The other twisted bilayer configuration usually show a rotation of ~ 30° (Figure 2d), which is believed to be the next lowest energy structure (1.6 eV/atom less stable than the AB stacked bilayer).[28] Atomic force microscopy (AFM) was employed to determine the thickness of the graphene films transferred onto silicon/silicon oxide substrate (Figure 2e–g). The central hexagonal contrast appears remarkably on the six-fold lobe. The height of the hexagonal second layer graphene with respect to the first layer six-fold lobe-like domain and the first layer graphene to the SiO_2 substrate are found to be ~ 0.34 nm and ~ 1.0 nm, respectively. The step height difference of 0.34 nm between the surface of first and second layer graphene is consistent with the ideal 0.335 nm of monolayer graphene. The larger thickness of the first layer on SiO_2 may be attributed to substrate-graphene spacing and contaminations resulted from the transfer process.

Since it is necessary to have an AB stacked bilayer graphene to achieve a tunable band gap under a vertical field, we have carried out a systematic study to investigate the dependence of the overall coverage and AB stacking ratio on various growth parameters such as H_2/CH_4 ratio, temperature, and pressure. High coverage of bilayer graphene can be obtained at a large range of H_2/CH_4 ratio (20–1400) (Figure S4 and S5), a relatively high growth temperature (1010–1050 °C) (Figure S6), and a relatively low pressure (2–20 mbar) (Figure S7 and S8). However, the AB stacking ratio appears to present a nearly invariable low value around 65 % under the growth conditions mentioned above. Importantly, our studies show that bilayer graphene with a higher yield of AB stacking ratio (up to 95 %) can be achieved at very low pressure (*e.g.* 1 mbar) (Figure S8) and high growth temperature (1030–1050 °C) (Figure S9). According to the Chapman-Enskog theory, the gas diffusion coefficient of the precursor can be promoted by higher growth temperature and lower pressure.[29] At the same time, the surface diffusion coefficient can also be increased with higher temperature. Therefore, high growth temperature and low pressure can provide enough free energy for the active carbon species to diffuse to the lowest energy state, which is favorable for achieving AB stacked bilayer graphene.

However, under this small window of growth conditions for high yield nucleation of AB stacked bilayer graphene seeds, the growth rate of the bilayer graphene is rather low (Figure S8). In this case, the Cu substrate is quickly totally covered by monolayer graphene during the initial 5 min growth and no catalytic active Cu gaps is left to provide carbon fragments for the continued growth of the second layer, resulting in a low overall coverage of the bilayer graphene (< 5 %) even after a relatively long duration of growth (*e.g.* 1 hour) (Figure 3b). To simultaneously obtain a high coverage and a high AB stacking ratio of bilayer graphene, we have adopted a two-step process with a low pressure nucleation step followed by a higher pressure growth step based on our systematic study described above: in step 1, a brief (*e.g.* 2 min) low pressure (1 mbar) growth at 1050 °C (H_2/CH_4 ratio of 40) was used to nucleate bilayer graphene seeds with high AB stacking ratio (Figure 3a); in step 2, the pressure was increased to a higher value (5 mbar) in order to increase the bilayer growth rate and therefore obtain a uniform high coverage bilayer graphene sheet in a 1 hour growth process (Figure 3c). Importantly, this change of growth conditions does not lead to apparent nucleation of new bilayer graphene domains, and therefore the original high AB stacking

ratio in bilayer graphene nuclei can be maintained. The coverage of bilayer graphene can be further increased by prolonging the growth time. Finally, nearly full coverage (~ 99 %) of bilayer graphene can be obtained after 3 hours of growth (Figure 3e).

Raman spectroscopy was employed to further characterize the quality of the bilayer graphene synthesized by the two-step process. The Raman spectra show very low intensity D band (around 1350 cm^{-1}, corresponding to disorder-induced defect) in the disoriented bilayer and essentially no D band signal in the AB stacked bilayer graphene (Figure 3f), suggesting the high quality of the bilayer graphene. We have further performed Raman spectroscopy measurements on more than 100 randomly chosen spots across. Histograms of 2D band FWHMs and I_{2D}/I_G ratio of the Raman spectra were then used to determine the AB stacking yield (Figure 3g and 3h). The observed FWHMs of 2D band are in the range of 47.5–62.0 cm^{-1} for the AB stacked bilayer graphene, 27.4–38.2 cm^{-1} for the disoriented bilayer graphene. The I_{2D}/I_G ratio is in the range of 0.83–1.46 for the AB stacked bilayer, and 3.45–4.77 for the disoriented bilayer. These statistical results are consistent with the previous reports that both the 2D band FWHMs and I_{2D}/I_G ratio can be used to determine the stacking order of the bilayer graphene.[12,30] Based on the histograms in Figure 3g, 3h, the AB stacked bilayer graphene consists of ~90 % of the total bilayer area (Figure 3i). Additional Raman mapping studies also confirms the high yield growth of AB stacked bilayer graphene (Figure S10).

High-resolution transmission electron microscopy (HRTEM) was further carried out to determine the thickness and quality of the graphene films synthesized by the two-step process. Obvious contrast between monolayer and bilayer graphene was observed after the sample was transferred onto a holy TEM grid (Figure 4a), where the lighter and darker regions indicated by blue and red circles correspond to the monolayer and bilayer graphene areas, respectively. Selected area electron diffraction (SAED) patterns (Figure 4b, c) corresponding to the monolayer and bilayer regions in Figure 4a, with the zone axis of [0001], show that the graphene is single crystalline, and the bilayer graphene is AB stacked. Diffraction intensity ratio of the outer {1–210} peak over the inner {−1100} peak in the profile plots show opposite trend for the mono- and bi-layer graphene (Figure 4e, f). Specifically, the ratio is close to 0.5 for the monolayer and approximately 2.0 for the bilayer graphene. These results agree well with the previous reports of AB-stacked bilayer graphene.[11,31] SAED pattern obtained from disoriented bilayer graphene typically shows the combination of two sets of diffraction spots with a ~ 30° rotation (Figure 4d).

To characterize the electronic quality of the bilayer graphene, we have carried out electrical transport studies on the single and dual-gated bilayer graphene devices (Figure 5a). The back-gate graphene devices are fabricated on silicon substrate with 300 nm silicon oxide. The resistance R *versus* the back-gated voltage (V_{BG}) (R-V_{BG}) plot shows typical ambipolar characteristics expected for the graphene devices (Figure 5b). Based on the transfer characteristics, the carrier mobility can be determined to be 3,700 cm^2/V·s using well developed procedures (also see the experimental section).[32,33] Electrical measurement over 50 devices demonstrates that the bilayer graphene exhibit excellent carrier mobilities in the range of 1,500–4,400 cm^2/V·s for holes (Figure 5c) and 1,400–3,000 cm^2/V·s for electrons, which is significantly better than the previously reported values of 350–580 cm^2/V·s for LPCVD bilayer graphene,[11,12] and comparable to those reported for exfoliated bilayer graphene (1,000 to 5,000 cm^2/V·s).[1,34]

To further probe the bilayer graphene characteristics under vertical displacement field, we have fabricated dual-gate bilayer graphene field-effect transistors (FETs). The dual-gate devices were fabricated with a transferred top-gate stack on the back-gated device (see method).[35] The two-dimensional plot of the device resistance R *vs.* top-gate voltage (V_{TG})

and V_{BG} shows that the highest resistance is achieved in the highest displacement field region (up-left and lower-right corners) (Figure 5d). This can be more evidently illustrated in a series of plots of R-V_{TG} at different V_{BG}. When sweeping the V_{TG} from −5 V to 3 V at different fixed V_{BG} from −80 V to 80 V, each R-V_{TG} curve shows maximum value R_{Dirac}, and the R_{Dirac} increases with increasing V_{BG} in both the positive and negative directions (Figure 5e). The plot of R_{Dirac} *vs.* displacement field further shows that maximum channel resistance are achieved under the highest displacement field (Figure 5f), confirming the AB stacking nature of the bilayer graphene.[2,11,12,36] This study clearly demonstrates that high quality bilayer graphene are obtained from the two-step synthesis process, which provides a rational route to grow large-area high quality AB stacked bilayer graphene.

CONCLUSION

High quality AB stacked bilayer graphene was successfully grown on Cu foils using a LPCVD approach. A high H_2/CH_4 ratio was employed to saturate graphene lateral growth as a result of equilibrium between growth and hydrogen etching, leaving catalytic active partially exposed Cu surface at the upstream end, which continuously generate active carbon fragments that flow downstream to enable the epitaxial growth of large-area bilayer graphene on the downstream monolayer. With a systematic study of the dependence of bilayer coverage and AB stacking order on the growth parameters, a two-step LPCVD process was developed to achieve a high AB stacking ratio in the large-area bilayer graphene. Electrical transport measurements showed that the optimized AB stacked bilayer graphene films exhibit a high electronic quality with the carrier mobility up to 4,400 cm^2/V·s at room temperature. This research should be beneficial for both the fundamental understanding of the bilayer graphene growth mechanism and for the development of functional graphene devices with tunable energy gaps.

EXPERIMENTAL SECTION

Graphene Growth

Graphene was synthesized by copper-catalyzed low pressure chemical vapor deposition (LPCVD) using a gas mixture of Ar, H_2, and CH_4, where CH_4 gas was the carbon-containing precursor. First, a 25-μm thick copper foils (99.8 %, Alfa Aesar) were washed with HCl/H_2O (1:10) and loaded into a 1-inch quartz tube inside a horizontal furnace (Lindberg/Blue M, Thermo Scientific). The system was evacuated to a vacuum of 20 mTorr for 10 min. Then, the growth chamber was filled with 500 sccm of Ar & H_2 mixed gas and heated to 1050 °C for the initial Cu cleaning for 30 min. Next, the diluted methane (500 ppm in Ar) was introduced into the tube for the graphene growth at 990–1050 °C with different H_2/CH_4 (pure) flow ratio (4–2666) under 1–100 mbar. The growth was terminated by quenching the quartz tube (cooling rate was approximately 200 °C/min) under ambient conditions.

Graphene Transfer

The transfer of the CVD-derived graphene films onto 300 nm SiO_2 substrates was performed by the wet-etching of the underlying Cu foils. Initially, the graphene was grown on both side of the copper foil. To transfer the graphene, one side of the Cu/graphene surface was spin-coated with PMMA (495 PMMA C2, MicroChem) photoresist and then cured at 120 °C for 2 min. The other side of the sample was exposed to O_2 plasma for 50 seconds to remove the graphene. The Cu foil was then etched away using copper etchant (Transene, CE-100), resulting in a free-standing PMMA/graphene membrane floating on the surface of the etchant bath. The PMMA/graphene film was washed with HCl/H_2O (1:10) and DI water for several times, and transferred onto a silicon substrate with 300 nm SiO_2.

Finally, the PMMA was dissolved by acetone and the substrate was rinsed with isopropyl alcohol to yield a graphene film on the substrate.

Characterization

The morphology and structure of the graphene were characterized with optical microscopy (OM, Olympus), field emission scanning electron microscopy (FESEM, JSM-6701F), high-resolution transmission electron microscopy (HRTEM, FEI Titan S/TEM at 300 kV), and Raman spectroscopy (Renishaw 1000, 514 nm laser wavelength, 50 × objective). The thickness was measured using atomic force microscopy (AFM, Veeco Dimension 5000).

Graphene Device Fabrication and Measurement

The electrical properties of the CVD bilayer graphene were characterized by fabricating back-gate and dual-gate graphene FET devices on 300 nm SiO_2 substrates. To this end, the as-grown bilayer graphene is first transferred onto the octadecyltrichlorosilane (OTS) modified Si/SiO_2 substrate. Photolithography and O_2 plasma etching were then used to pattern graphene films into 7.5 μm strips. E-beam lithography was then employed to pattern the contact electrodes with the channel lengths of 7.5 μm. The source/drain electrodes were deposited using e-beam evaporation (Ti/Au: 50 nm/50 nm). The back gate voltage was applied by using a Si back gate with SiO_2 as the dielectric. For the dual gate device, the top-gate was fabricated with a transferred gate stack to minimize the potential damage to graphene channel during the dielectric integration process.[33,35,37,38] For transferring gate stack, a 50 nm gold thin film is deposited on a Si/SiO_2 substrate using e-beam evaporation. An Al_2O_3 top-gate dielectrics film is then deposited on gold surface by atomic layer deposition (ALD) at 250 °C. E-beam lithography and e-beam evaporation was then used to define metal strips (Ti/Au: 20/40 nm). The Al_2O_3 top-gate dielectrics film is then patterned by anisotropic reactive-ion etching (RIE) using e-beam patterned metal strips as the etching mask to form metal-dielectrics stack structure. A thin layer of AZ4620 photoresist is then spin coated onto the substrate to wrap around the gate stack. A thermal release tape (TRT) is attached onto the top of the substrate. Then the whole structure is immersed in deionized (DI) water at room temperature, followed by the peeling-off of an edge of the TRT. The gold layer is etched away using gold etchant. Then the TRT and the attached top-gate structure are laminated onto patterned graphene strips. A peeling off process is operated at the glassy transition point of the photoresist followed by repeated acetone rinse in order to remove the photoresist. *E*-beam lithography and e-beam vacuum metallization (Ti/Au, 50/50 nm) are then used to define the source, drain and gate electrodes. Electrical transport properties of the samples were measured in a vacuum probe station (Lakeshore Model TTP4) at room temperature using dual-gate FETs configuration and a computer-controlled analogue-to-digital converter (National Instruments model 6030E). To extract the mobility, the total resistance of the device can be expressed as below: [32,33]

$$R_{tot} = R_{contact} + R_{channel} = R_{contact} + \frac{L/W}{ne\mu}$$

Where $R_{channel}$ is the resistance of the graphene channel, $R_{contact}$ is the contact resistance of the metal/graphene contact, L is the channel length, W is the channel width, and n is the carrier concentration in the graphene channel region, and can be approximated by the following equation:

$$n = \sqrt{n_0^2 + n_{BG}^2} = \sqrt{n_0^2 + (C_{BG}(V_{BG} - V_{Dirac})/e)^2}$$

Where n_0 is the residual carrier concentration, representing the density of carriers at Dirac point. $n_{BG} = C_{BG} \times (V_{BG} - V_{Dirac})/e$ is the carrier concentration induced by the back-gate bias away from the Dirac point. C_{BG} can be approximated by the oxide capacitance.[32]

By fitting this model to the measured data, we can extract the relevant parameters, n_0, $R_{contact}$ and μ. We use y $a + b \times (1 + c \times x)^{-1/2}$ fitting the measured data.

$$n_0 = \frac{C_{BG}/e}{\sqrt{c}}; \quad R_{contact} = a; \quad \mu = \frac{(L/W) \times \sqrt{c}}{b \times C_{BG}}$$

Supplementary Material

Refer to Web version on PubMed Central for supplementary material.

Acknowledgments

REFERENCES AND NOTES

1. Zhang Y, Tang TT, Girit C, Hao Z, Martin MC, Zettl A, Crommie MF, Shen YR, Wang F. Direct Observation of a Widely Tunable Bandgap in Bilayer Graphene. Nature. 2009; 459:820–823. [PubMed: 19516337]

2. Xia F, Farmer DB, Lin Y, Avouris P. Graphene Field-Effect Transistor with High On/Off Ratio and Large Transport Band Gap at Room Temperature. Nano Lett. 2010; 10:715–718. [PubMed: 20092332]

3. Geim AK, Novoselov KS. The Rise of Graphene. Nat Mater. 2007; 6:183–191. [PubMed: 17330084]

4. Castro EV, Novoselov KS, Morozov SV, Peres NMR, Lopes dos Santos JMB, Nilsson J, Guinea F, Geim AK, Castro Neto AH. Biased Bilayer Graphene: Semiconductor with a Gap Tunable by the Electric Field Effect. Phys Rev Lett. 2007; 99:216802–216805. [PubMed: 18233240]

5. Ohta T, Bostwick A, Seyller T, Horn K, Rotenberg E. Controlling the Electronic Structure of Bilayer Graphene. Science. 2006; 313:951–954. [PubMed: 16917057]

6. Dillenschneider R, Han JH. Exciton Formation in Graphene Bilayer. Phys Rev B. 2008; 78:045401–945409.

7. Park JU, Nam SW, Lee MS, Lieber CM. Synthesis of Monolithic Graphene-Graphite Integrated Electronics. Nat Mater. 2012; 11:120–125. [PubMed: 22101813]

8. Alstrup I, Chorkendorff I, Ullmann S. The Interaction of CH_4 at High Temperatures with Clean and Oxygen Precovered Cu(100). Surface Science. 1992; 264:95–102.

9. Oshima C, Nagashima A. Ultra-Thin Epitaxial Films of Graphite and Hexagonal Boron Nitride on Solid Surface. J Phys : Condens Matter. 1997; 9:1–20.

10. Reina A, Jia X, Ho J, Nezich D, Son H, Bulovic V, Dresselhaus MS, Kong J. Large Area, Few-Layer Graphene Films on Arbitrary Substrates by Chemical Vapor Deposition. Nano Lett. 2009; 9:30–35. [PubMed: 19046078]

11. Lee S, Lee K, Zhong Z. Wafer Scale Homogeneous Bilayer Graphene Films by Chemical Vapor Deposition. Nano Lett. 2010; 10:4702–4707. [PubMed: 20932046]

12. Yan K, Peng H, Zhou Y, Li H, Liu Z. Formation of Bilayer Bernal Graphene: Layer-by-Layer Epitaxy *via* Chemical Vapor Deposition. Nano Lett. 2011; 11:1106–1110. [PubMed: 21322597]

13. Peng Z, Yan Z, Sun Z, Tour JM. Direct Growth of Bilayer Graphene on SiO_2 Substrates by Carbon Diffusion through Nickel. ACS Nano. 2011; 5:8241–8247. [PubMed: 21888426]

14. Yan Z, Peng Z, Sun Z, Yao J, Zhu Y, Liu Z, Ajayan PM, Tour JM. Growth of Bilayer Graphene on Insulating Substrates. ACS Nano. 2011; 5:8187–8192. [PubMed: 21888396]

15. Chen Z, Ren W, Liu B, Gao L, Pei S, Wu ZS, Zhao J, Cheng HM. Bulk Growth of Mono-to Few-Layer Graphene on Nickel Particles by Chemical Vapor Deposition from Methane. Carbon. 2010; 48:3543–3550.

16. Zeng Z, Huang X, Yin Z, Li H, Chen Y, Li H, Zhang Q, Ma J, Boey F, Zhang H. Fabrication of Graphene Nanomesh by Using an Anodic Aluminum Oxide Membrane as a Template. Adv Mater. 201210.1002/adma.201104281

17. Kim KS, Zhao Y, Jang H, Lee SY, Kim JM, Kim KS, Ahn JH, Kim P, Choi JY, Hong BH. Large-Scale Pattern Growth of Graphene Films for Stretchable Transparent Electrodes. Nature. 2009; 457:706–710. [PubMed: 19145232]

18. Chen Z, Ren W, Gao L, Liu B, Pei S, Cheng HM. Three-Dimensional Flexible and Conductive Interconnected Graphene Networks Grown by Chemical Vapor Deposition. Nat Mater. 2011; 10:424–428. [PubMed: 21478883]

19. Gao L, Ren W, Xu H, Jin L, Wang Z, Ma T, Ma LP, Zhang Z, Fu Q, Peng LM, et al. Repeated Growth and Bubbling Transfer of Graphene with Millimetre-Size Single-Crystal Grains Using Platinum. Nature Communications. 2012; 3:699–705.

20. Li X, Cai W, An J, Kim S, Nah J, Yang D, Piner R, Velamakanni A, Jung I, Tutuc E, et al. Large-Area Synthesis of High-Quality and Uniform Graphene Films on Copper Foils. Science. 2009; 324:1312–1314. [PubMed: 19423775]

21. Bae S, Kim H, Lee Y, Xu X, Park JS, Zheng Y, Balakrishnan J, Lei T, Kim HR, Song Y, et al. Roll-to-Roll Porduction of 30-Inch Graphene Films for Transparent Electrodes. Nat Nanotechnol. 2010; 5:574–578. [PubMed: 20562870]

22. Huang PY, Ruiz-Vargas CS, Zande AM, Whitney WS, Levendorf MP, Kevek JW, Garg S, Alden JS, Hustedt CJ, Zhu Y, et al. Grains and Grain Boundaries in Single-Layer Graphene Atomic Patchwork Quilts. Nature. 2011; 469:389–392. [PubMed: 21209615]

23. Chen S, Cai W, Piner RD, Suk JW, Wu Y, Ren Y, Kang J, Ruoff RS. Synthesis and Characterization of Large-Area Graphene and Graphite Films on Commercial Cu-Ni Alloy Foils. Nano Lett. 2011; 11:3519–3525. [PubMed: 21793495]

24. Zhang W, Wu P, Li Z, Yang J. First-Principles Thermodynamics of Graphene Growth on Cu Surfaces. J Phys Chem C. 2011; 115:17782–17787.

25. Vlassiouk I, Regmi M, Fulvio P, Dai S, Datskos P, Eres G, Smirnov S. Role of Hydrogen in Chemical Vapor Deposition Growth of Large Single-Crystal Graphene. ACS Nano. 2011; 5:6069–6076. [PubMed: 21707037]

26. Li X, Magnuson CW, Venugopal A, An J, Suk JW, Han B, Borysiak M, Cai W, Velamakanni A, Zhu Y, Fu L, et al. Graphene Films with Large Domain Size by a Two-Step Chemical Vapor Deposition Process. Nano Lett. 2010; 10:4328–4334. [PubMed: 20957985]

27. Liu L, Zhou H, Cheng R, Chen Y, Lin YC, Qu Y, Bai J, Ivanov IA, Liu G, Huang Y, et al. A Systematic Study of Atmospheric Pressure Chemical Vapor Deposition Growth of Large-Area Monolayer Graphene. J Mater Chem. 2012; 22:1498–1503.

28. Shallcross S, Sharma S, Pankratov OA. Twist boundary in graphene: energetics and electric field effect. J Phys : Condens Matter. 2008; 20:454224–454228.

29. Cussler, EL. Diffusion: Mass Transfer in Fluid System. New York: Cambridge university press; 1997.

30. Robertson AW, Warner JH. Hexagonal Single Crystal Domains of Few-Layer Graphene on Copper oils. Nano Lett. 2011; 11:1182–1189. [PubMed: 21322599]

31. Meyer JC, Geim AK, Katsnelson MI, Novoselov KS, Booth TJ, Roth S. The Structure of Suspended Graphene Sheets. Nature. 2007; 446:60–63. [PubMed: 17330039]

32. Kim S, Nah J, Jo I, Shahrjerdi D, Colombo L, Yao Z, Tutuc E, Banerjee SK. Realization of a High Mobility Dual-Gated Graphene Field-Effect Transistor with Al_2O_3 Dielectric. Appl Phys Lett. 2009; 94:062107–062109.

33. Liao L, Bai J, Qu Y, Lin YC, Li Y, Huang Y, Duan X. High-k Oxide Nanoribbons as Gate Dielectrics for High Mobility Top-Gated Graphene Transistors. PNAS. 2010; 107:6711–6715. [PubMed: 20308584]

34. Zou K, Zhu J. Transport in Gapped Bilayer Graphene: The Role of Potential Fluctuations. Phys Rev B. 2010; 82:081407–081410.

35. Cheng R, Bai J, Liao L, Zhou H, Chen Y, Liu L, Lin YC, Jiang S, Huang Y, Duan X. High-Frequency Self-Aligned Graphene Transistor with Transferred Gate Stacks. PNAS. 2012; 109:11588–11592. [PubMed: 22753503]

36. Yu WJ, Liao L, Chae SH, Lee YH, Duan X. Toward Tunable Band Gap and Tunable Dirac Point in Bilayer Graphene with Molecular Doping. Nano Lett. 2011; 11:4759–4763. [PubMed: 21985035]

37. Lee B, Park SY, Kim HC, Cho KJ, Vogel EM, Kim MJ, Wallace RM, Kim J. Confomal Al_2O_3 Dielectric Layer Deposited by Atomic Layer Deposition for Graphene-Based Nanoelectronics. Appl Phys Lett. 2008; 92:203102–203104.

38. Wang X, Tabakman SM, Dai H. Atomic Layer Deposition of Metal Oxides on Pristine and Functionalized Graphene. J Am Chem Soc. 2008; 130:8152–8153. [PubMed: 18529002]
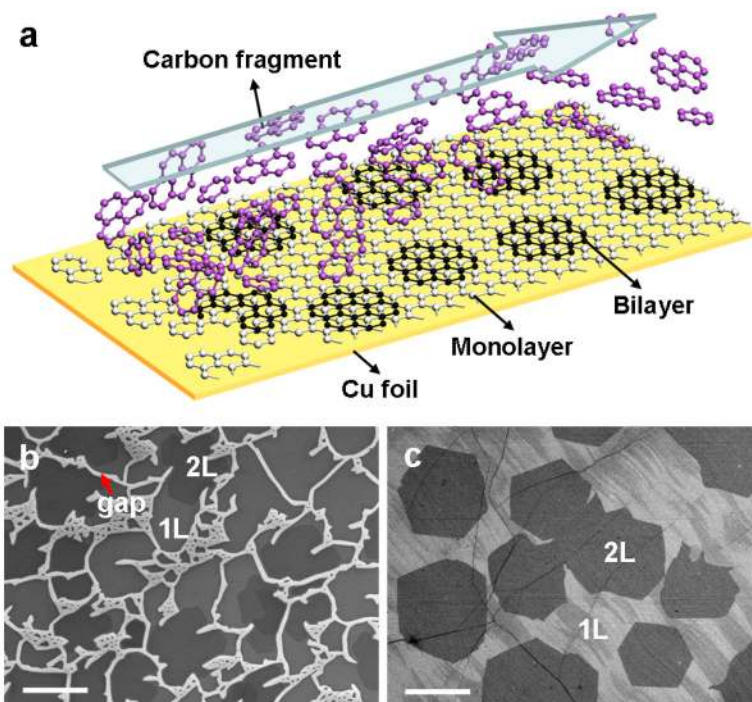
Figure 1.
(a) A schematic illustration of the bilayer graphene growth. Carbon fragments come from the uncovered upstream Cu catalyst are continuously transported downstream for the growth of bilayer graphene. (b, c) SEM images of monolayer (1L) and bilayer (2L) graphene at upstream end and center of the Cu substrate, respectively. The bright strips in b are the exposed copper surface between graphene domains, and the darker hexagonal contrast corresponds to the bilayer graphene. Scale bars are 20 μm.
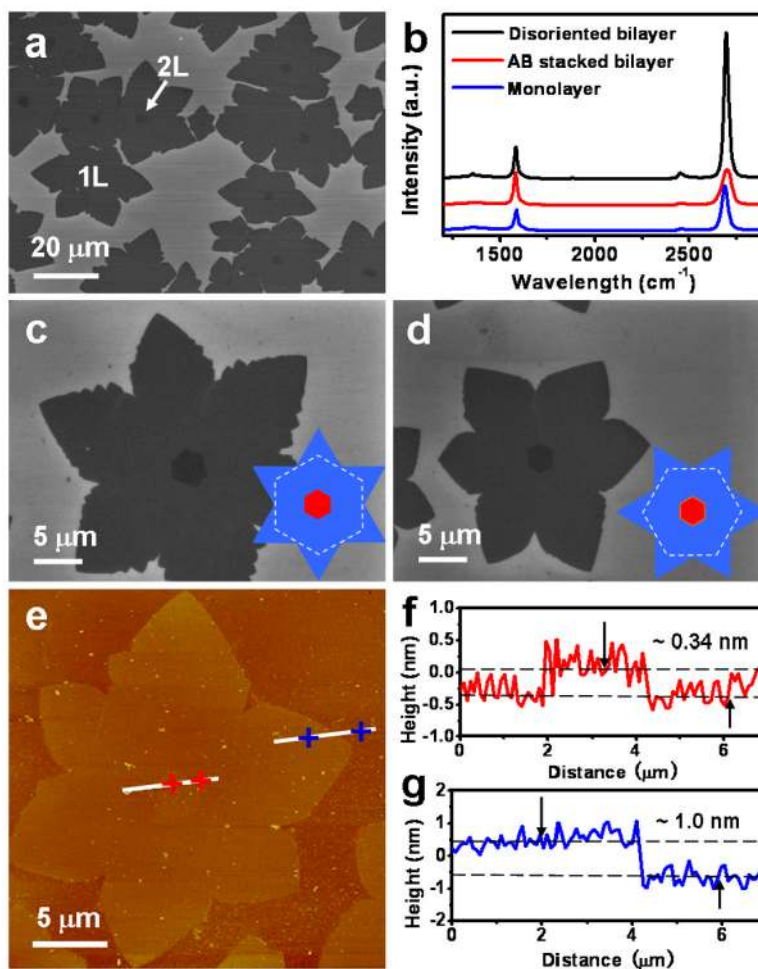
Figure 2.
(a) SEM image of the initial monolayer (1L) and bilayer (2L) graphene domains transferred onto SiO$_2$/Si substrate synthesized in a 2-min growth with H$_2$/CH$_4$ ratio of 40 under 5 mbar at 1050 °C. The hexagonal bilayer domains are typically located at the centers of the monolayer domains. (b) Raman spectra of the monolayer and bilayer graphene. Bilayer graphene is presented by two different stacking arrangements: AB stacking and disoriented stacking. (c) and (d) Enlarged SEM images of the AB stacked and disoriented bilayer graphene domains, respectively. The insets are the schematic diagrams for the two different stacking orders. (e) AFM image of a graphene domain on SiO$_2$ substrate. The two white lines near center and edge of the domain indicate the sections corresponding to the depth profiles shown in (f) and (g). The height difference between the two dashed lines is ~ 0.34 nm in (f) and ~ 1.0 nm in (g), respectively.
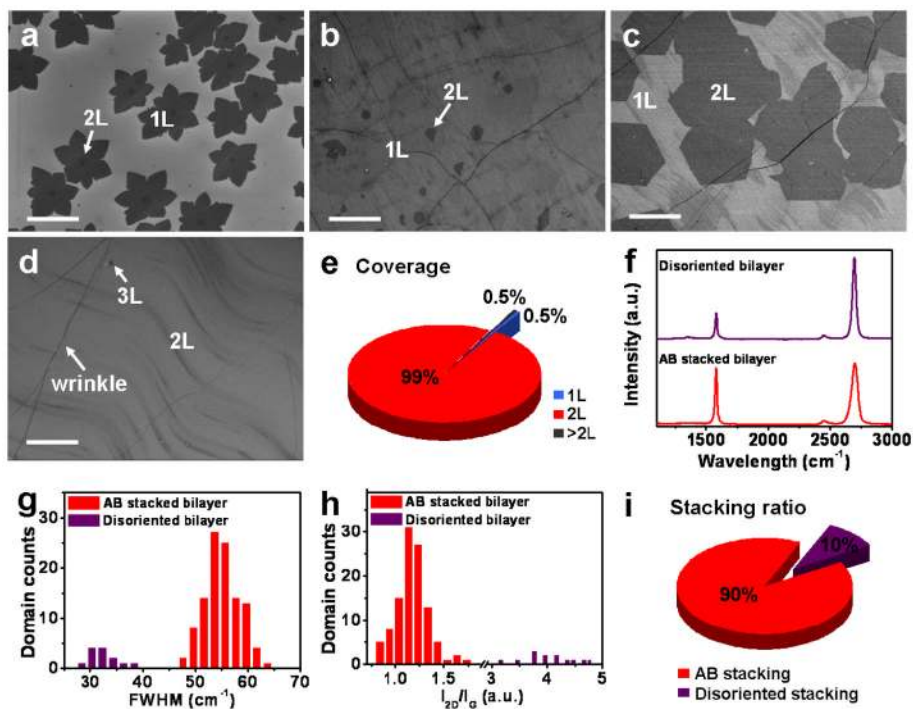
Figure 3.
SEM images of monolayer and bilayer graphene on the center of Cu foil synthesized with H_2/CH_4 ratio of 40 under 1 mbar at 1050 °C for (a) 2 min and (b) 1 hour growth. (c) SEM image shows that the bilayer graphene coverage is increased dramatically by increasing pressure to 5 mbar for 1 hour growth after the first 2 min low pressure nucleation step. (d) SEM image of higher coverage of bilayer graphene obtained after extending the growth duration to 3 hours. Scale bars are 20 µm. (e) Coverage statistics of different layers for the sample shown in (d) demonstrates that ~ 99 % of surface area is covered by bilayer graphene. (f) Representative Raman spectra of the two different stacked bilayer graphene in (d). (g, h) Histograms of the Raman spectrum 2D band FWHMs and I_{2D}/I_G ratio of the bilayer graphene. (i) Stacking ratio statistics of the bilayer graphene based on (g, h).
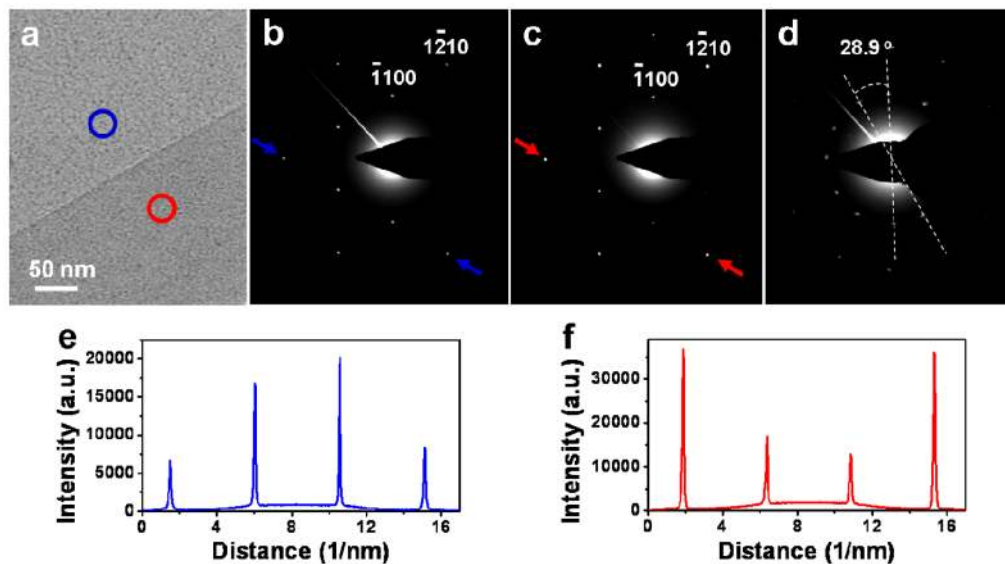
Figure 4.
(a) HRTEM image of graphene synthesized by the two-step process, suspended on a holey carbon TEM grid. The monolayer and bilayer regions are marked by the blue and red circles. (b, c) SAED patterns of monolayer and AB stacked bilayer graphene regions in (a), respectively. (d) SAED pattern obtained from disoriented bilayer graphene, showing two sets of diffraction spots with a 28.9° rotation. (e, f) Profile plots of diffraction peak intensities along arrows in (b and (c), respectively.
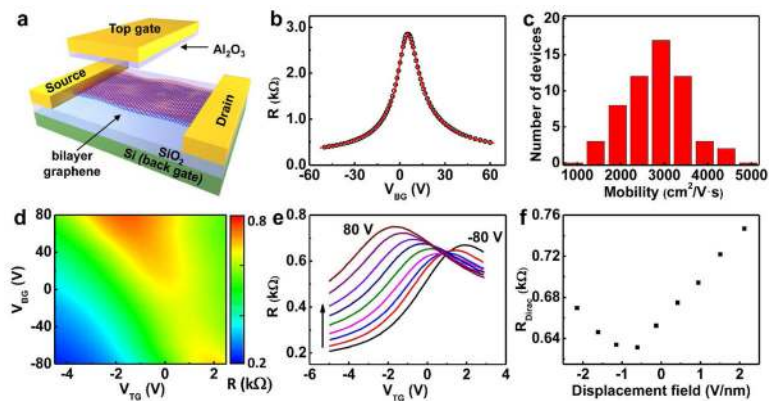
Figure 5.
(a) Schematic illustration of bilayer graphene device with single back-gate or dual-gate. (b) Device resistance *v.s.* back gate voltage (V_{BG}). The hollow circles represent experimental data point and red line is the modeling fit to extract carrier mobility. (c) Histogram of the carrier (hole) mobility distribution for back-gated bilayer graphene devices. The devices studied in b and c have a channel length of 7.5 µm and width of 7.5 µm. (d) 2D plot of R_{total} as functions of both top gate voltage (V_{TG}) and V_{BG} of a dual-gate bilayer graphene device. (e) A series of R *v.s.* V_{TG} curves at different value of fixed V_{BG} ranging from −80 to 80 V, with 20 V increment. (f) Resistance at Dirac point under different displacement field.